A Hamiltonian Approach to the Eikonal Equation

Kaleem Siddiqi[1], Allen Tannenbaum[2], and Steven W. Zucker[3]

[1]School of Computer Science & Center for Intelligent Machines
McGill University, 3480 University Street, Montréal, PQ, Canada H3A 2A7.

[2]Department of Electrical and Computer Engineering
University of Minnesota, 200 Union Street S. E. Minneapolis, MN 55455.

[3]Department of Computer Science & Center for Computational Vision & Control
Yale University, New Haven, CT 06520-8285.

Abstract. The eikonal equation and variants of it are of significant interest for problems in computer vision and image processing. It is the basis for continuous versions of mathematical morphology, stereo, shape-from-shading and for recent dynamic theories of shape. Its numerical simulation can be delicate, owing to the formation of singularities in the evolving front, and is typically based on level set methods introduced by Osher and Sethian. However, there are more classical approaches rooted in Hamiltonian physics, which have received little consideration in the computer vision literature. Here the front is interpreted as minimizing a particular action functional. In this context, we introduce a new algorithm for simulating the eikonal equation, which offers a number of computational advantages over the earlier methods. In particular, the locus of shocks is computed in a robust and efficient manner. We illustrate the approach with several numerical examples.

1 Introduction

Variational principles emerged naturally from considerations of energy minimization in mechanics [11]. We consider these in the context of the eikonal equation, which arises in geometrical optics and, recently, which has become of great interest for problems in computer vision [4]. It is the basis for continuous versions of mathematical morphology [3, 16, 24, 25], as well as for Blum's grassfire transform [2] and new dynamic theories of shape representation including [9, 22, 21]. It has also been widely used for applications in image processing and analysis [17, 5], shape-from-shading [10] and stereo [8].

The numerical simulation of this equation is non-trivial, because it is a hyperbolic partial differential equation for which a smooth initial front may develop singularities or *shocks* as it propagates. At such points, classical concepts such as the normal to a curve, and its curvature, are not defined. Nevertheless, it is precisely these points that are important for the above applications in computer

vision since, e.g., it is they which denote the skeleton (see Figures 4 and 5). To continue the evolution while preserving shocks, the technology of level set methods introduced by Osher and Sethian [14], has proved to be extremely powerful. The approach relies on the notion of a weak solution, developed in viscosity theory [6, 12], and the introduction of an appropriate entropy condition to select it. Care must be taken to use an upwind scheme to compute derivatives, so that information is not blurred across singularities. The representation of the evolving front as a level set of a hypersurface allows topological changes to be handled in a natural way, and robust, efficient implementations have recently been developed [18].

Level set methods are Eulerian in nature because computations are restricted to grid points whose locations are fixed. For such methods, the question of computing the locus of shocks for dynamically changing systems remains of crucial importance, i.e., the methods are shock *preserving* but do not explicitly *detect* shocks. One approach, such as that taken in [20], is to rely on one-sided interpolation of the underlying hypersurface between grid points, to provide sub-pixel estimates of the singularities. Such methods suffer the disadvantage that the interpolation step is computationally very expensive, and introduces numerical thresholds for shock detection. Hence, in order to obtain satisfactory results, high order accurate numerical schemes must be used to simulate the evolving front [13].

On the other hand, there are more classical methods rooted in Hamiltonian physics, which can also be used to study shock theory. To the best of our knowledge, these have not been considered in the computer vision literature. The purpose of this paper is to introduce these methods and a straightforward algorithm for simulating the eikonal equation. The approach offers a number of computational advantages, in particular, the locus of shocks is computed in a robust and efficient manner. The proposed algorithm is Lagrangian in nature, i.e., the front is explicitly represented as a sequence of marker particles. The motion of these particles is then governed by an underlying Hamiltonian system. Such systems are of course fundamental in classical physics, and the technique we elucidate for shock tracking therefore has a natural physical interpretation based on elementary Hamiltonian and Lagrangian mechanics.

2 The Eikonal Equation

We begin by showing the connection between a monotonically advancing front, and the well known eikonal equation. Consider the curve evolution equation

$$\frac{\partial \mathcal{C}}{\partial t} = F\mathcal{N}, \tag{1}$$

where $\mathcal{C}$ is the vector of curve coordinates, $\mathcal{N}$ is the unit inward normal, and $F = F(x, y)$ is the speed of the front at each point in the plane, with $F \geq 0$ (the case $F \leq 0$ is also allowed). Let $T(x, y)$ be a graph of the solution surface, obtained by superimposing all the evolved curves in time (see Figure 1). In other

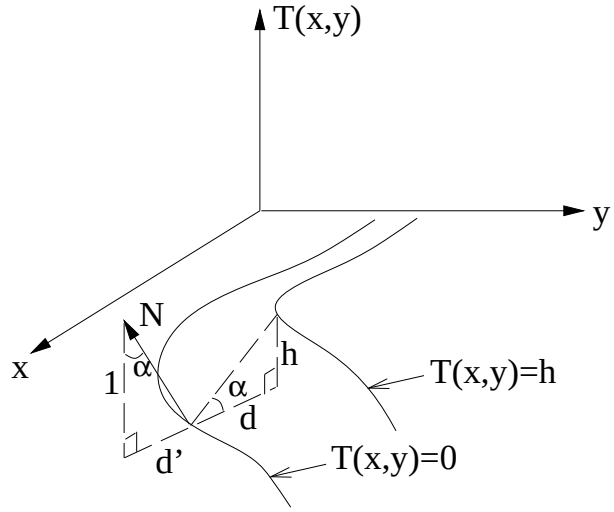

Fig. 1. A geometric view of a monotonically advancing front (Eq. 1). $T(x, y)$ is a graph of the 'solution' surface, the level sets of which are the evolved curves.

words, $T(x, y)$ is the time at which the curve crosses a point (x, y) in the plane. Referring to the figure, the speed of the front is given by

$$F(x, y) = \frac{d}{h} = \frac{1}{\tan(\alpha)} = \frac{1}{d'} = \frac{1}{\|\nabla T\|}.$$

Hence, $T(x, y)$ satisfies the *eikonal equation*

$$\|\nabla T\| \, F = 1. \tag{2}$$

A number of algorithms have been recently developed to solve a quadratic form of this equation, i.e., $\|\nabla T\|^2 = \frac{1}{F^2}$. These include Sethian's fast marching method [18], which relies on an interpretation of Huygens's principle to efficiently propagate the solution from the initial curve, and Rouy and Tourin's viscosity solutions approach [15]. However, neither of these methods address the issue of shock detection explicitly, and more work has to be done to track shocks.

A different approach, which is related to the solution surface $T(x, y)$ viewed as a graph, has been proposed by Shah *et al* [19, 22]. Here the key idea is to use an edge strength functional v in place of the surface $T(x, y)$, computed by a linear diffusion equation. The framework provides an approximation to the reaction-diffusion space introduced in [9]. However, it does not extend to the extreme cases, i.e., morphological erosion by a disc structuring element (reaction) or motion by curvature (diffusion). Hence, points of maximum (local) curvature are interpreted as skeletal points, and the framework provides a type of regularized skeleton. Its relation to the classical skeleton, obtained from the eikonal equation with $F = 1$, is as yet unclear. For example, the curvature maxima based skeleton

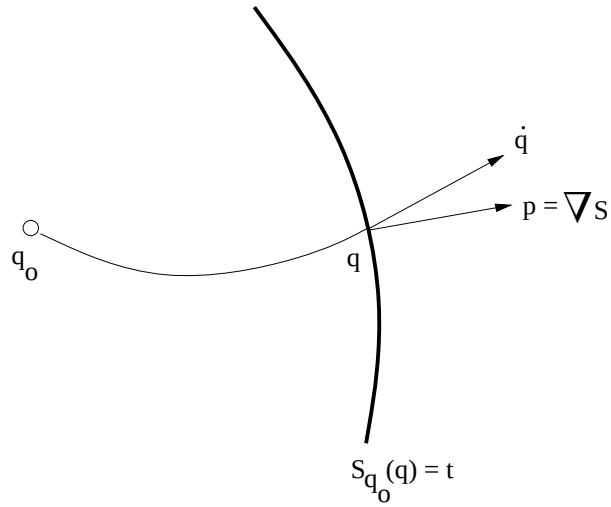

Fig. 2. Direction of a ray $\dot{\mathbf{q}}$ and the direction of motion of the wave front $\mathbf{p}$. From [1].

may not be connected (see the examples in [19, 22]). Nevertheless, the framework is computationally very efficient since the governing equation is linear and can be implemented using finite central differences. Furthermore, it can be applied directly to greyscale images as well as to curves with triple point junctions.

In the next section, we shall consider an alternate framework for solving the eikonal equation, which is based on the canonical equations of Hamilton. The technique is widely used in classical mechanics, and rests on the use of a Legendre transformation (see [1] for the precise definition) which takes a system of n second-order differential equations to a (mathematically equivalent) system of $2n$ first-order differential equations. We believe that for a number of vision problems involving shock tracking and skeletonization, this represents a natural way of implementing the eikonal equation.

3 Hamilton's Canonical Equations

Following Arnold [1, pp. 248–258], we shall use Huygens' principle to show the connection between the eikonal equation and the Hamilton-Jacobi equation. For every point $\mathbf{q}_0$, define the function $S_{\mathbf{q}_0}(\mathbf{q})$ as the optical length of the path from $\mathbf{q}_0$ to $\mathbf{q}$ (see Figure 2). The wave front at time t is given by $\{\mathbf{q} : S_{\mathbf{q}_0}(\mathbf{q}) = t\}$. The vector $\mathbf{p} = \frac{\partial S}{\partial \mathbf{q}}$ is called the *vector of normal slowness of the front.* By Huygens' principle the direction of the ray $\dot{\mathbf{q}}$ is conjugate to the direction of motion of the front, i.e., $\mathbf{p} \cdot \dot{\mathbf{q}} = 1$. Note that these directions do not coincide in an anisotropic medium.

Let us specialize to the case of a monotonically advancing front in an inhomogeneous but isotropic medium (Eq. 1). Here the speed $F(x, y)$ depends only

on position (not on direction), and the directions of $\mathbf{p}$ and $\dot{\mathbf{q}}$ coincide. The action function minimized, $S(\mathbf{q}, t)$, is defined as

$$S_{\mathbf{q}_0, t_0}(\mathbf{q}, t) = \int_\gamma L dt,$$

along the extremal curve γ connecting the points $(\mathbf{q}_0, t_0)$ and $(\mathbf{q}, t)$. Here the Lagrangian

$$L = \frac{1}{F(x, y)} \|\partial\gamma/\partial t\|$$

is a conformal (infinitesimal) length element, and we have assumed that the extremals emanating from the point $(\mathbf{q}_0, t_0)$ do not intersect elsewhere, i.e., they form a *central field of extremals.* Note that for an isotropic medium the extremals are straight lines, and that for the special case $F(x, y) = 1$, the action function becomes Euclidean length.

It can be shown that the vector of normal slowness, $\mathbf{p} = \frac{\partial S}{\partial \mathbf{q}}$, is not arbitrary but satisfies the Hamilton-Jacobi equation

$$\frac{\partial S}{\partial t} = -H\left(\frac{\partial S}{\partial \mathbf{q}}, \mathbf{q}\right), \tag{3}$$

where the Hamiltonian function $H(\mathbf{p}, \mathbf{q})$ is the Legendre transformation with respect to $\dot{\mathbf{q}}$ of the Lagrangian function $L(\mathbf{q}, \dot{\mathbf{q}})$. Rather than solve the nonlinear Hamilton-Jacobi equation for the action function S (which will give the solution surface $T(x, y)$ to Eq. 2), it is much more convenient to look at the evolution of the phase space $(\mathbf{p}, \mathbf{q})$ under the equivalent Hamiltonian system

$$\dot{\mathbf{p}} = -\frac{\partial H}{\partial \mathbf{q}}, \qquad \dot{\mathbf{q}} = \frac{\partial H}{\partial \mathbf{p}}.$$

This offers a number of advantages, the most significant being that the equations become linear, and hence trivial to simulate numerically. In the following we shall derive this system of equations for the special case of a front advancing with speed $F(x, y) = 1$.

4 The Hamilton-Jacobi Skeleton Flow

For the case of a front moving with constant speed, recall that the action function being minimized is Euclidean length, and hence S can be viewed as a Euclidean distance function from the initial curve $\mathcal{C}_0$. Furthermore, the magnitude of its gradient, $\|\nabla S\|$, is identical to 1 in its smooth regime, which is precisely where the assumption of a central field of extremals is valid.

With $\mathbf{q} = (x, y)$, $\mathbf{p} = (S_x, S_y)$, associate to the evolving plane curve $\mathcal{C} \subset \mathbf{R}^2$ the surface $\tilde{C} \subset \mathbf{R}^4$ given by

$$\tilde{C} := \{(x, y, S_x, S_y) : (x, y) \in C,\ S_x^2 + S_y^2 = 1,\ \mathbf{p} \cdot \dot{\mathbf{q}} = 1\}.$$

The Hamiltonian function obtained by applying a Legendre transformation to the Lagrangian $L = \|\dot{\mathbf{q}}\|$ is given by

$$H = \mathbf{p} \cdot \dot{\mathbf{q}} - L = 1 - (S_x^2 + S_y^2)^{\frac{1}{2}}.$$

The associated Hamiltonian system is:

$$\dot{\mathbf{p}} = -\frac{\partial H}{\partial \mathbf{q}} = (0,0), \qquad \dot{\mathbf{q}} = \frac{\partial H}{\partial \mathbf{p}} = -(S_x, S_y). \tag{4}$$

Evolve $\tilde{C}$ under this system of equations and let $\tilde{C}(t) \subset \mathbf{R}^4$ denote the resulting (contact) surface. Now project $\tilde{C}(t)$ to $\mathbf{R}^2$ to get the parallel evolution of $\mathcal{C}$ at time t, $\mathcal{C}(t)$.

5 Numerical Simulations

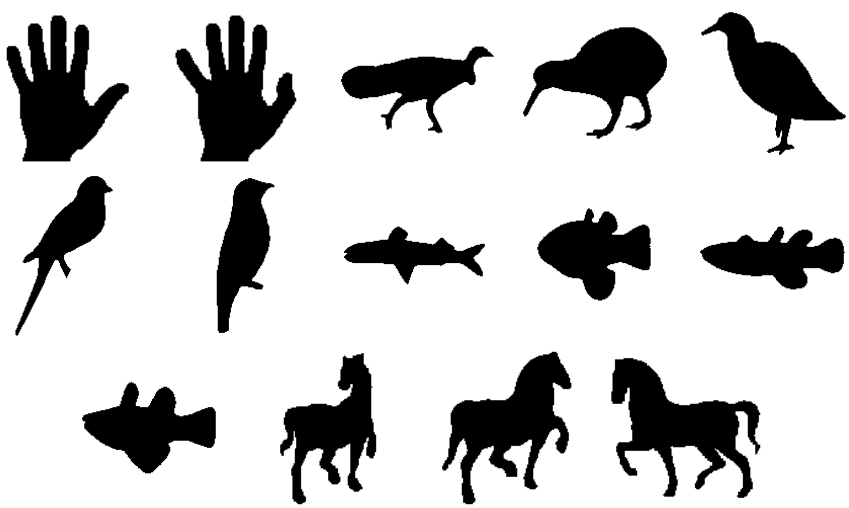

Fig. 3. The original binary shapes used in our experiments range in size from 128x128 to 168x168 pixels^2.

In this section we apply the above theory to formulate an efficient algorithm for simulating the eikonal equation, while tracking the shocks which form. Recall that since the approach is a Lagrangian one, marker particles will have to first be placed along the initial curve, which in our simulations is assumed to be a simple closed curve in the plane.[1] The evolution of marker particles is then governed

[1] The method also extends naturally to a set of open curves by interpreting S as an outward distance function from the collection of curve segments. The initial marker particles are placed on the boundaries of an infinitesimal dilation of each open curve, and are then evolved in an outward direction.

by Eq. 4. With $\mathbf{q} = (x, y)$, $\mathbf{p} = (S_x, S_y) = \nabla S$, the system of equations

$$\dot{S}_x = 0, \dot{S}_y = 0; \qquad \dot{x} = -S_x, \dot{y} = -S_y$$

gives a gradient dynamical system. The second equation indicates that the trajectory of the marker particles will be governed by the vector field obtained from the gradient of the Euclidean distance function S, and the first indicates that this vector field does not change with time, and can be computed once at the beginning of the simulation. Projecting this 4D system onto the (x, y) plane for each instance of time t will give the evolved curve $\mathcal{C}(t)$.

In order to obtain accurate results, three numerical issues need to be addressed. First, in order to obtain a dense sequence of marker particles, a continuous representation of the initial shape's boundary ($T(x, y) = 0$, see Figure 1) is needed. Second, it is possible for marker particles to drift apart in rarefaction regions, i.e., concave portions of the curve may fan out. Hence, new marker particles must be interpolated when necessary. Third, whereas finite central differences are adequate for estimating the gradient of the Euclidean distance function in its smooth regime, such estimates will lead to errors near singularities, where S is not differentiable. Hence, we use ENO interpolants for estimating derivatives [13]; the key idea is to obtain information from the "smooth" side, in the vicinity of a singularity. The algorithm may now be stated as follows:

1. Take as the initial curve $T(x(s), y(s)) = 0$, the given boundary of an object, assumed to be a simple closed curve in the plane.
2. Create an ordered sequence of marker particles at positions Δs apart along the boundary.
3. Compute a Euclidean distance transform, where each grid point in the interior of the boundary is assigned its Euclidean distance to the closest marker particle.
4. For each grid point in the interior of the boundary compute and store the components of the vector field ∇S, using ENO interpolants.

5. Do for **step** from **0** to **TOTALSTEPS** {
  Do for **particle** from **0** to **NPARTICLES** {
    - Update the particle's position based on
      ∇S at the closest grid point:
      $x(step + 1) = x(step) - \Delta t \times S_x$,
      $y(step + 1) = y(step) - \Delta t \times S_y$
    - **if** (Distance(particle,next_particle) $> a\Delta s$){
      interpolate a new particle in between.
    }
  }
}

The original binary shapes used in our experiments are depicted in Figure 3. The simulations are based on a piecewise circular arc representation of the boundary, obtained using the contour tracer developed in [20] on the signed distance transform of the original shape. Prior to obtaining the contour, the

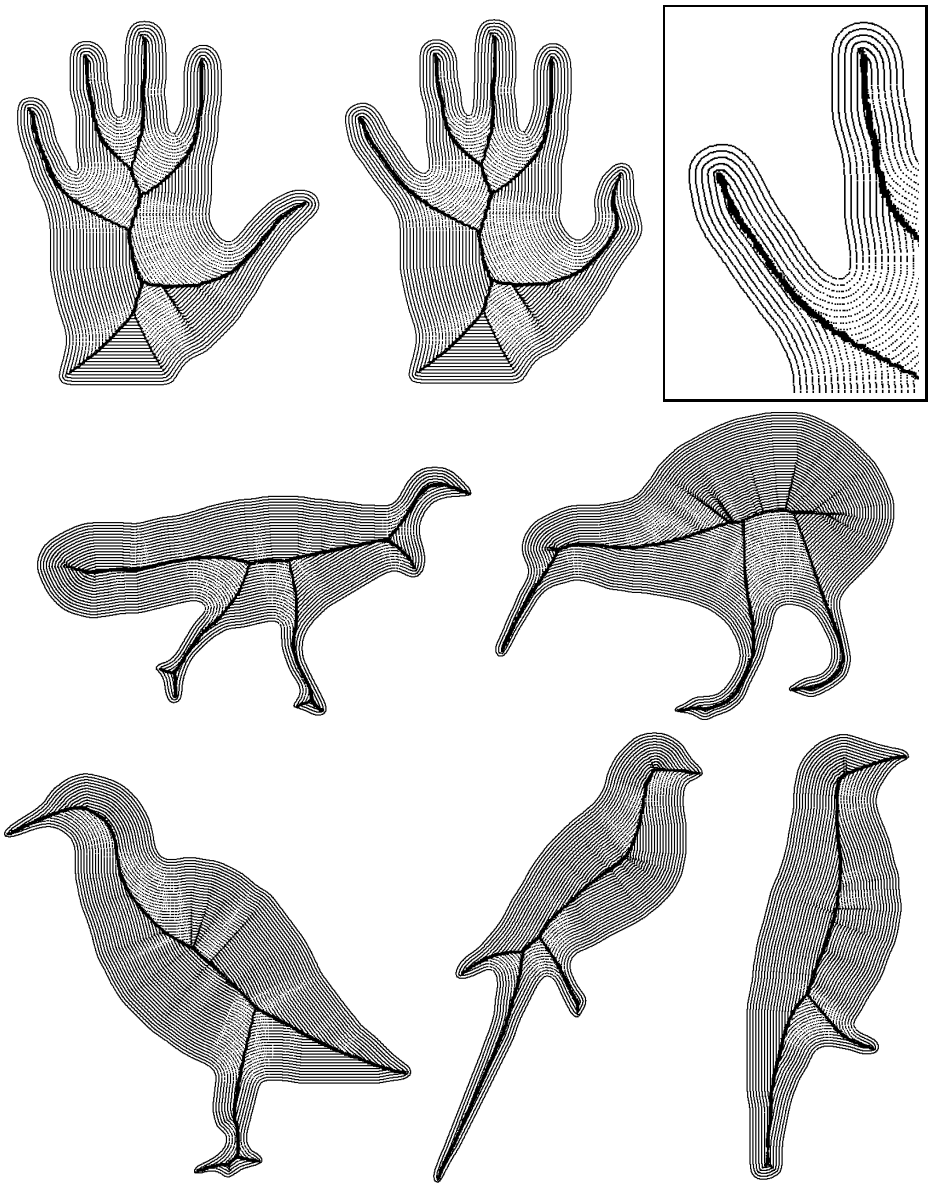

Fig. 4. The evolution of marker particles under the Hamiltonian system. The initial particles are placed on the boundary, and iterations of the process are superimposed. These correspond to level sets of the solution surface $T(x, y)$ in Figure 1. Individual marker particles are more clearly visible in the zoom-in on the fingers of the hand (top right). See Section 5 for a discussion.

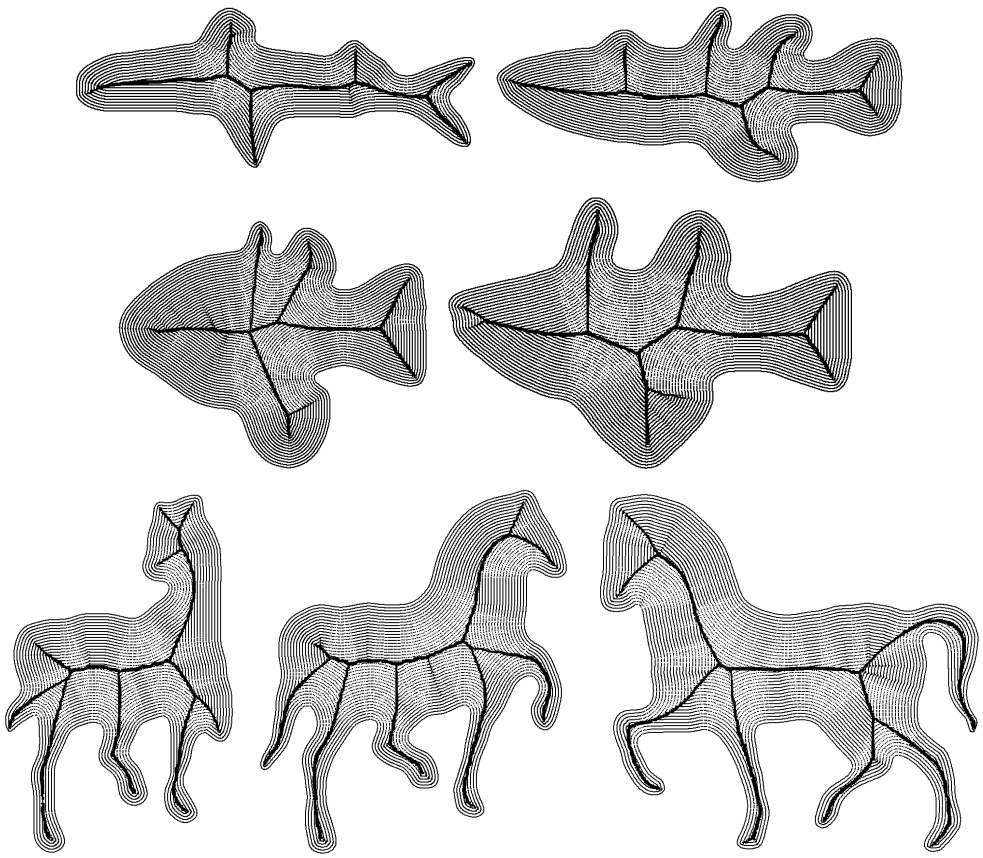

Fig. 5. The evolution of marker particles under the Hamiltonian system. The initial particles are placed on the boundary, and iterations of the process are superimposed. Each iteration gives a level set of the solution surface $T(x, y)$ in Figure 1. See Section 5 for a discussion.

distance transform is Gaussian blurred very slightly ($\sigma = 0.5$ pixels) to combat discretization. The birth of new marker particles (step 5) is also based on circular arc interpolation. Figures 4 and 5 depict the evolution of marker particles, with speed $F = 1$, for several different shapes. For all simulations, the spacing Δs of initial marker particles is 0.25 pixels, the spacing criterion for interpolating a new particle in the course of the evolution is $a\Delta s = 0.75$ pixels, and the resolution of the Euclidean distance transform S is the same as that of the original binary image. The timestep Δt is 0.5 pixels, and results for every second iteration are saved. The superposition of all the level curves gives the solution surface $T(x, y)$ in Figure 1. It is important to note that in principle higher order interpolants can be used for the placement of marker particles, and the resolution of the exact distance transform is not limited by that of the original binary shape.

The results are comparable to those obtained using higher order ENO implementations, although the algorithm is computationally more efficient (linear in the number of marker particles). Informal timing experiments indicate that the efficiency of the algorithm exceeds that of level set methods, except under the "fast marching" implementation, with which it compares favorably. However, when shock detection is included, the Hamiltonian approach has important conceptual and computational advantages. In particular, in contrast with level set approaches, topological splits are not explicitly handled, but shocks (collisions of marker particles) are. In effect, the marker particles are jittered back and forth along the crest lines of the distance function S, leading to thick traces.

The above simulation of the eikonal equation has a variety of applications in computer vision [4, 9, 22, 21, 10, 8], mathematical morphology [3, 16, 24, 25], and image processing and analysis [17, 5]. If desired, it is also possible to formulate an explicit stopping condition for the marker particles. The key idea is to consider the net outward flux per unit volume of the vector field underlying the Hamiltonian system, and to detect locations where energy is lost. As a bi-product of this analysis, which will be described in future work, the skeleton can be robustly and efficiently obtained using only local parallel computations. Figure 6 illustrates the potential of this method, on the same set of shapes. These results may be interpreted as a "stopping potential"; as marker particles enter the regime of negative flux (shown in white) they can be extinguished.

6 Conclusions

In this paper we have introduced a new algorithm for simulating the eikonal equation. The method is rooted in Hamiltonian physics and offers a number of computational advantages when it comes to shock tracking. In future work we plan to extend our results to 3D, where the underlying Hamiltonian system will have the same structure, and the same divergence analysis can be carried out. However, the placement and interpolation of marker particles on the propagating surface will be more delicate. In closing, we note that in related recent work, vector fields rooted in magneto-statics have been used for extracting symmetry and edge lines in greyscale images [7], and that a wave propagation framework

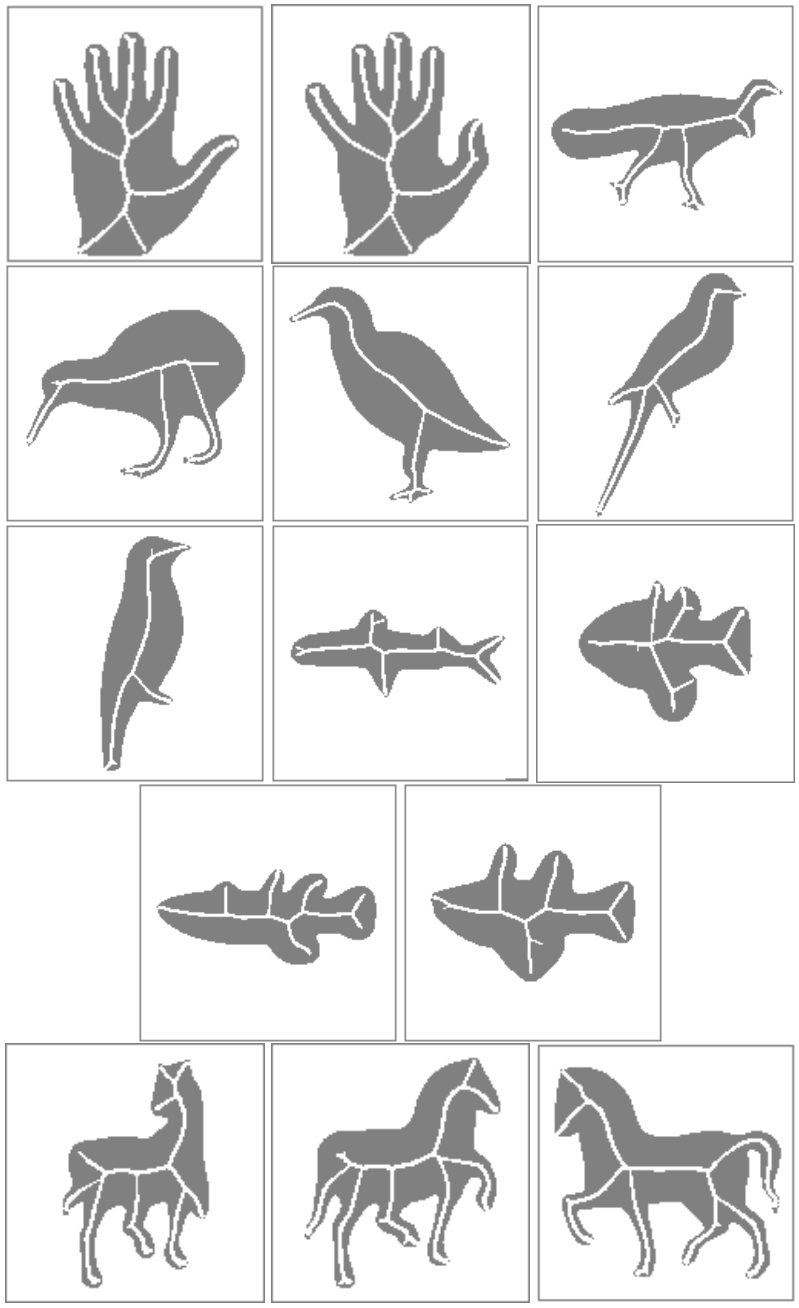

Fig. 6. A divergence-based skeleton, superimposed in white on the original binary shapes (shown in grey). Comparing with the Hamiltonian system based flows in Figures 4 and 5, these maps can be used to formulate a explicit stopping condition for the individual marker particles.

on a discrete grid has been proposed for curve evolution and mathematical morphology [23].

Acknowledgements This work was supported by the Natural Sciences and Engineering Research Council of Canada, the National Science Foundation, the Air Force Office of Scientific Research, the Army Research Office and by a Multi University Research Initiative grant.

References

1. V. Arnold. *Mathematical Methods of Classical Mechanics, Second Edition.* Springer-Verlag, 1989.
2. H. Blum. Biological shape and visual science. *J. Theor. Biol.*, 38:205–287, 1973.
3. R. Brockett and P. Maragos. Evolution equations for continuous-scale morphology. In *Proceedings of the IEEE Conference on Acoustics, Speech and Signal Processing*, San Francisco, CA, March 1992.
4. A. R. Bruss. The eikonal equation: Some results applicable to computer vision. In B. K. P. Horn and M. J. Brooks, editors, *Shape From Shading*, pages 69–87, Cambridge, MA, 1989. MIT Press.
5. V. Caselles, J.-M. Morel, G. Sapiro, and A. Tannenbaum, editors. *IEEE Transactions on Image Processing, Special Issue on PDEs and and Geometry-Driven Diffusion in Image Processing and Analysis*, 1998.
6. M. G. Crandall, H. Ishii, and P.-L. Lions. User's guide to viscosity solutions of second order partial differential equations. *Bulletin of the American Mathematical Society*, 27(1):1–67, 1992.
7. A. D. J. Cross and E. R. Hancock. Scale-space vector fields for feature analysis. In *Conference on Computer Vision and Pattern Recognition*, pages 738–743, June 1997.
8. O. Faugeras and R. Keriven. Complete dense stereovision using level set methods. In *Fifth European Conference on Computer Vision*, volume 1, pages 379–393, 1998.
9. B. B. Kimia, A. Tannenbaum, and S. W. Zucker. Shape, shocks, and deformations I: The components of two-dimensional shape and the reaction-diffusion space. *International Journal of Computer Vision*, 15:189–224, 1995.
10. R. Kimmel, K. Siddiqi, B. B. Kimia, and A. Bruckstein. Shape from shading: Level set propagation and viscosity solutions. *International Journal of Computer Vision*, 16(2):107–133, 1995.
11. C. Lanczos. *The Variational Principles of Mechanics.* Dover, 1986.
12. R. J. LeVeque. *Numerical Methods for Conservation Laws.* Birkhauser Verlag, 1992.
13. S. Osher and C.-W. Shu. High-order essentially non-oscillatory schemes for Hamilton-Jacobi equations. *SIAM Journal of Numerical Analysis*, 28:907–922, 1991.
14. S. J. Osher and J. A. Sethian. Fronts propagating with curvature dependent speed: Algorithms based on hamilton-jacobi formulations. *Journal of Computational Physics*, 79:12–49, 1988.
15. E. Rouy and A. Tourin. A viscosity solutions approach to shape-from-shading. *SIAM. J. Numer. Analy.*, 29(3):867–884, June 1992.
16. G. Sapiro, B. B. Kimia, R. Kimmel, D. Shaked, and A. Bruckstein. Implementing continuous-scale morphology. *Pattern Recognition*, 26(9), 1992.

17. J. Sethian. *Level Set Methods: evolving interfaces in geometry, fluid mechanics, computer vision, and materials science.* Cambridge University Press, Cambridge, 1996.
18. J. A. Sethian. A fast marching level set method for monotonically advancing fronts. *Proc. Natl. Acad. Sci. USA*, 93:1591–1595, February 1996.
19. J. Shah. A common framework for curve evolution, segmentation and anisotropic diffusion. In *Conference on Computer Vision and Pattern Recognition*, pages 136–142, June 1996.
20. K. Siddiqi, B. B. Kimia, and C. Shu. Geometric shock-capturing eno schemes for subpixel interpolation, computation and curve evolution. *Graphical Models and Image Processing*, 59(5):278–301, September 1997.
21. K. Siddiqi, A. Shokoufandeh, S. J. Dickinson, and S. W. Zucker. Shock graphs and shape matching. *International Journal of Computer Vision*, to appear, 1999.
22. Z. S. G. Tari, J. Shah, and H. Pien. Extraction of shape skeletons from grayscale images. *Computer Vision and Image Understanding*, 66:133–146, May 1997.
23. H. Tek and B. B. Kimia. Curve evolution, wave propagation and mathematical morphology. In *Fourth International Symposium on Mathematical Morphology*, June 1998.
24. R. van den Boomgaard. Mathematical morphology: extensions towards computer vision. Ph.D. dissertation, University of Amsterdam, March 1992.
25. R. van den Boomgaard and A. Smeulders. The morphological structure of images: The differential equations of morphological scale-space. *IEEE Transactions on Pattern Analysis and Machine Intelligence*, 16(11):1101–1113, November 1994.